Structural and Spectroscopic Investigations of LaFeAl$_{11}$O$_{19}$ Compounds

E. TRONC, F. LAVILLE, M. GASPERIN,* A. M. LEJUS, AND D. VIVIEN

*Laboratoire de Chimie Appliquée de l'Etat Solide (UA 302, CNRS), ENSCP, 11 rue P. et M. Curie, 75231 Paris Cedex 05, France, and *Laboratoire de Minéralogie-Cristallographie (UA 09, CNRS), UPMC, 4 Place Jussieu, 75252 Paris Cedex 05, France*

Single crystals of nonstoichiometric LaFeAl$_{11}$O$_{19}$, isotypic with magnetoplumbite, have been prepared. Structural refinement and investigations by ESR and optical and Mössbauer spectroscopies have been performed. It is deduced that iron is in the 2+ state, and that Fe^{2+} ions are localized in the tetrahedral sites of the spinel blocks. By air annealing, Fe^{2+} is partially converted into Fe^{3+}. A significant amount of Fe^{3+} ions appears in trigonal bipyramidal sites. © 1989 Academic Press, Inc.

Introduction

Trivalent lanthanide hexaaluminates LnMAl$_{11}$O$_{19}$, isotypic with magnetoplumbite (Pb^{2+}Fe$_{12}^{3+}$O$_{19}$), are interesting for their optical properties and their use as lasers or luminescent materials (*1, 2*). Nonsubstituted compounds have quite a narrow existence range (*3*). They are difficult to prepare even at high temperature. They have a distorted framework with vacancies both on cationic and anionic sublattices (*4*), and are generally described by the formula Ln^{3+}Al$_{11}^{3+}$O$_{18}$. The introduction of M^{2+} ions in the lattice stabilizes the structure which can thus be obtained at room temperature. These materials have the general formula $Ln^{3+}M^{2+}$Al$_{11}$O$_{19}$ where Ln = La to Gd (*5*), M = Mg (*5–7*), Mn (*7*), Fe, Co, Ni, Cu (*8*). Previous investigations (*4*) have shown that

the position of the M^{2+} ions in the lattice can vary with their nature and their amount. In order to precise the charge compensation mechanism, structural and spectroscopic investigations on LaFeAl$_{11}$O$_{19}$ and its oxidation have been performed; they are reported here.

Crystal Growth and Characterization

Crystals corresponding to formal compositions LaFeAl$_{11}$O$_{19}$ and LaFe$_{0.5}$Mg$_{0.5}$Al$_{11}$O$_{19}$ have been obtained using the flame fusion method (Verneuil process) as detailed elsewhere (*4, 8*). The starting material was an intimate mixture of powdered oxides γ-Al$_2$O$_3$, La$_2$O$_3$, and α-Fe$_2$O$_3$ (and MgO) in stoichiometric amounts. The reducing power of the oxyhydrogen torch was adjusted in order to convert Fe^{3+} into Fe^{2+}.

The samples were rod-shaped, 8–10 mm in diameter, 20–30 mm long. They consisted of large crystals with a pink color characteristic of Fe^{2+}. The skin of the Verneuil boules, however, looked yellow-brown as a result of surface oxidation by air during the cooling step at the end of the growth process. Annealing in air at 1500°C made the crystal color change from pink to ocher, indicating the presence of Fe^{3+} in significant amount.

Debye–Scherrer powder diagrams of as-grown and annealed crystals confirmed the magnetoplumbite-type structure. The lattice parameters are given in Table I. The crystals cleaved into platelets perpendicular to the **c** direction; the growth axis was the **a** direction. Despite a strong mosaic character, large areas (a few millimeters) of very good crystalline quality (Laue test) were obtained. For each compound, a batch of wafers was selected and ground for use in spectroscopic investigations.

Chemical analyses were performed using the electron microprobe. In every case, the results (Table I) indicated a slight loss in La and a significant loss in Fe with respect to the initial composition. Effective compositions actually remain uncertain since nonstoichiometry can result from cationic and anionic vacancies.

Crystal Structure Refinement

The magnetoplumbite ($PbFe_{12}O_{19}$) structure, with space group $P6_3/mmc$, can be described by the packing $RSR*S*$ where R and S blocks have the composition (Pb^{2+} $Fe_6^{3+}O_{11}$)$^{2-}$ and ($Fe_6^{3+}O_8$)$^{2+}$, respectively. The $*$ means that the block has been turned 180° around the **c** axis.

In $LaMAl_{11}O_{19}$ (4), La^{3+} substitutes for Pb^{2+} while M^{2+} and Al^{3+} ions are distributed over the Fe^{3+} sites. The stacking is schematically represented in Fig. 1. Per unit formula, there are two tetrahedral (Al$_2$), nine octahedral (1 Al$_1$, 6 Al$_4$, 2 Al$_3$),

TABLE I

SAMPLE CHARACTERISTICS

Formula	Analysis[a] La : Fe : Mg : Al	Parameters	
		a (Å)	c (Å)
LaFeAl$_{11}$O$_{19}$	0.79 : 0.50 : — : 11	5.586	22.017
Annealed in air 1500°C	0.86 : 0.65 : — : 11	5.596	22.060
LaFe$_{0.5}$Mg$_{0.5}$Al$_{11}$O$_{19}$	0.83 : 0.30 : 0.37 : 11	5.587	21.998

[a] The results are based on 10 independent measurements per sample. Uncertainties are ca. ±0.03.

and one bipyramidal (Al$_5$) sites. Deviations from the ideal structure are systematically found in the La-aluminates (4), which are:

—off-center shift of atoms La (partial change in Wyckoff position 2d → 6h), Al$_5$ (2b → 4e, with location at one of the two pseudotetrahedral sites of the bipyramid), and also, in LaAl$_{11}$O$_{18}$, a displacement of oxygen atoms O$_1$ (6h → 12j) and O$_2$ (12k → 24l); statistical occupation of the sites consequently leads to occupancy factors lowered from 1 to $\frac{1}{3}$ or $\frac{1}{2}$;

—vacancies of atoms in the mirror plane (La, Al$_5$, O$_1$) and, in addition, at the junction of R and S blocks (Al$_4$) in LaAl$_{11}$O$_{18}$.

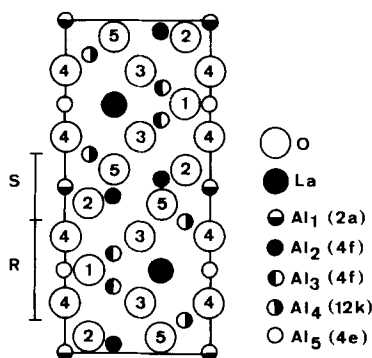In order to determine the Fe^{2+} ion location in LaFeAl$_{11}$O$_{19}$, the structural refine-

FIG. 1. (110) plane of LaFeAl$_{11}$O$_{19}$.

TABLE II

STRUCTURAL PARAMETERS OF $LaFeAl_{11}O_{19}$

Site	Wyckoff notation	Occupancy factor total (Fe^{2+})	Coordinates			B (Å²)
			$x \times 10^4$	$y \times 10^4$	$z \times 10^4$	
La_1	2d	0.83	6667	3333	2500	0.5(6)
La_2	6h	0.045	7241(6)	4481	2500	0.4(9)
Al_1	2a	1 (0.05)	0	0	0	0.3(6)
Al_2	4f	1 (0.25)	3333	6667	275(1)	0.2(5)
Al_3	4f	1 (0.08)	3333	6667	1898(1)	0.4(6)
Al_4	12k	1 (0.05)	8322(1)	6643	1082(1)	0.3(6)
Al_5	4e	0.5 (0)	0	0	2404(1)	0.5(9)
O_1	6h	1	1819(4)	3638	2500	0.5(0)
O_2	12k	1	1527(2)	3053	529(1)	0.4(7)
O_3	12k	1	5044(2)	87	1504(1)	0.2(8)
O_4	4e	1	0	0	1497(2)	0.3(7)
O_5	4f	1	6667	3333	576(2)	0.3(7)

ment was performed using a single crystal prepared under stoichiometric conditions. X-ray data were collected with a Philips PW 1100 diffractometer equipped with a graphite monochromator to select the MoKα radiation, and using a $\theta/2\theta$ scanning with a speed of 0.025°/sec. Nine hundred eighty-four independent reflections were retained after Lorentz-polarization corrections. Data were corrected for secondary extinction (0.585 × 10^{-5}). Absorption corrections were neglected ($\mu r < 1$). Atomic parameters of $LaMnAl_{11}O_{19}$ (4) were taken as starting values. The composition was assumed to be stoichiometric because of the low accuracy of the chemical analysis and of correlations between occupancy factors.

First adjustments of La^{3+} parameters were achieved with a statistical distribution of Fe^{2+} over all Al sites. Then, the coordinates and isotropic temperature factors of the other ions were allowed to vary. It resulted that the thermal factor at the Al_5 (4e) site increased notably; it became negative at the Al_2 (4f) site whereas the other sites were little affected. It was deduced that the Al_5 site was free of Fe^{2+} while the Al_2 site was enriched in Fe^{2+}. The Fe^{2+} and Al^{3+}

distribution over the various sites was then adjusted with the help of Fourier and difference Fourier maps. The final set of parameters ($R = 0.07$) is listed in Table II. Main interatomic distances are given in Table III.

Since no account was taken of deviations from stoichiometry, occupancy factors given in Table II are only indicative. Nevertheless, they clearly indicate the preferential localization of Fe^{2+} ions in the Al_2 tetrahedral sites of the S blocks. The finding of small amounts of Fe^{2+} spread in the octahedral sites (Al_1, Al_3, Al_4) and not in the pseudotetrahedral bipyramidal sites (Al_5) shows only that the electron density is lower in the latter. In fact, Fe^{2+} ions may not be present in the octahedral sites while some bipyramidal sites are vacant.

The comparison with data reported for $LaAl_{11}O_{18}$ (4) shows that whereas the splitting of cations (La, Al_5) persists in $LaFeAl_{11}O_{19}$ that of oxygen atoms (O_1, O_2) no longer occurs. It is indicative of improved long-range ordering, as also supported by considerable weakening of the diffuse scattering pattern (4). Interatomic distances (Table III) exhibit little variation except at

TABLE III

INTERATOMIC DISTANCES (Å) IN LaFeAl$_{11}$O$_{19}$: COMPARISON WITH THEIR
EQUIVALENTS IN LaAl$_{11}$O$_{18}$ (4) (GIVEN IN BRACKETS)

La-polyedra	La$_1$–O$_1$ (×6) 2.797 (2.779)	$\langle$La$_1$–O$\rangle$ = 2.747 (2.741)
	–O$_3$ (×6) 2.697 (2.703)	
	–Al$_5$ (×3) 3.232 (3.214)	
	La$_2$–O$_1$ (×2) 2.823	La$_2$–Al$_5$ (×2) 3.542
	–O$_1$ (×2) 2.351	–Al$_5$ (×1) 2.678
	–O$_1$ (×2) 3.301	
	–O$_3$ (×2) 3.054	
	–O$_3$ (×4) 2.591	
Al$_1$-octahedron	Al$_1$–O$_2$ (×6) 1.881 (1.885)	
Al$_2$-tetrahedron	Al$_2$–O$_2$ (×3) 1.832 (1.791)	$\langle$Al$_2$–O$\rangle$ = 1.843 (1.797)
	–O$_5$ (×1) 1.874 (1.813)	
Al$_3$-octahedron	Al$_3$–O$_1$ (×3) 1.976 (1.976)	$\langle$Al$_3$–O$\rangle$ = 1.922 (1.923)
	–O$_3$ (×3) 1.869 (1.870)	
Al$_4$-octahedron	Al$_4$–O$_2$ (×2) 1.975 (2.014)	$\langle$Al$_4$–O$\rangle$ = 1.907 (1.919)
	–O$_3$ (×2) 1.838 (1.838)	
	–O$_4$ (×1) 1.863 (1.842)	
	–O$_5$ (×1) 1.951 (1.965)	
Al$_5$-bipyramid	Al$_5$–O$_1$ (×3) 1.773 (1.763)	$\langle$Al$_5$–O$\rangle_{tet}$ = 1.829 (1.821)
	–O$_4$ (×1) 1.997 (1.994)	
	–O$_4$ (×1) 2.420 (2.496)	$\langle$Al$_5$–O$\rangle_{bipyr}$ = 1.947 (1.996)
	–Al$_5$ (×1) 0.423 (0.502)	

the Al$_2$ and Al$_5$ sites. The presence of Fe^{2+} in the structure significantly increases the average Al–O distance at the Al$_2$ site (1.84 against 1.80 Å), consistently with partial Fe^{2+} fitting. The average Al–O distance at the Al$_5$ bipyramidal site decreases from 2.00 to 1.95 Å, which is solely due to the short-ening of the O$_4$–O$_4$ distance (from 4.49 to 4.42 Å) and may result from increased oc-cupancy of the site.

In order to detect anomalies in bond lengths, we have calculated the apparent valence of the various atoms. We used the relationship (9)

$$s_{ij} = \exp[(r_0 - d_{ij})/0.37],$$

where s_{ij} is the valence of the bond between the atoms i and j, d_{ij} is the bond length, and r_0 is a parameter characteristic of the atomic pair. The apparent valence of the atom i is obtained by summing s_{ij} over the j neighbors. The expected value is the oxida-tion state. Higher or lower values indicate

bond lengths, respectively, shorter or longer than normal.

Valence sums are given in Table IV, along with data calculated from (4) for La Al$_{11}$O$_{18}$. The La (6h) ions have been omit-ted for the sake of simplicity. Both sets are

TABLE IV

APPARENT VALANCES IN LaFeAl$_{11}$O$_{19}$ AND IN
LaAl$_{11}$O$_{18}$ (GIVEN IN PARENTHESES)

r_0(La^{3+}) = 2.172	r_0(Al^{3+}) = 1.651	r_0(Fe^{2+}) = 1.734			
La$_1$	Al$_1$	Al$_2$	Al$_3$	Al$_4$	Al$_5$
2.56	3.22	2.43^a	2.91	3.05	2.67
(2.59)	(3.19)	(2.70)	(2.90)	(2.98)	(2.72)
O$_1$	O$_2$	O$_3$	O$_4$	O$_5$	
1.93	2.02	2.00	1.95	1.91	
(1.96)	(1.97)	(2.00)	(2.04)	(1.93)	

^{a} Assuming a site population of 1 Al^{3+}. Influence of Fe^{2+} occupation given in the text.

similar except for the (Al_2) tetrahedral sites of the S blocks, which supports preferential occupation by Fe^{2+} ions. The apparent valence of Al^{3+} in $LaAl_{11}O_{18}$ is equal to 2.70. Since the site is probably fully occupied, the valence reduction (10%) is attributed to underbonded Al^{3+} ion. This seems typical of aluminates with the magnetoplumbite and β-alumina structures (*10*) where the apparent valence of the Al_2 site is consistently close to 2.66. It is still lower in $LaFeAl_{11}O_{19}$ if population exclusively by Al^{3+} is assumed. Partial filling by Fe^{2+} reduces the discrepancy between observed and expected values. The bond valence increases and the average charge decreases. Assuming the same bond lengths, the deviation is equal to 8% for a Fe^{2+} population of 25% and vanishes for 38% (average charge = 2.62). This stresses that partial replacement of Al^{3+} ions by Fe^{2+} ions, larger and more polarizable, does not produce important distortions and that it improves the tetrahedral bonding. The La and Al_5 bipyramidal ions also show significant valence reduction. It may either result from some site distortions or from underoccupation, oxygen atoms relaxing around a vacancy leading to an apparently expanded site.

ESR Spectra

ESR spectra were recorded at room temperature on a Bruker ER 220D X-band spectrometer.

The ESR spectrum (Fig. 2a) of $LaFeAl_{11}O_{19}$ is mainly characterized by a broad asymmetrical line centered at $g = 2$ and a weak line at $g = 4.3$. Since Fe^{2+} ions are not seen by ESR spectroscopy at room temperature, both signals are attributed to Fe^{3+} present as traces in the material.

After annealing (Fig. 2b), the line at $g = 2$ is slightly increased (by about 10%). In the low field region, the line at 4.2 is much enhanced (its magnitude is eight times larger),
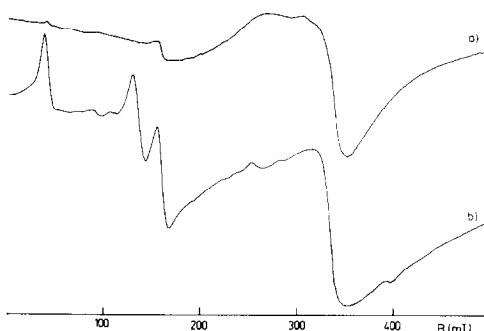

FIG. 2. ESR spectra of $LaFeAl_{11}O_{19}$, as-grown (a) and annealed in air at 1500°C (b).

and two new lines appear at $g \sim 4.9$ and 15.8.

Generally, signals at $g \sim 4.3$ and 2 are assigned to Fe^{3+} ($S = \frac{5}{2}$) ions in tetrahedral and octahedral sites, respectively (*11, 12*). Magnetically interacting Fe^{3+} ions can also give rise to signals at about $g = 2$ (*11*).

Assignment of the lines at $g = 4.9$ and 15.8 is more problematic. As soon as the site symmetry is lowered with respect to T_d or O_h, the splitting of the fundamental term $^6S_{5/2}$ becomes important, and transitions can arise over a wide field range (*13, 14*). Lines whose position is weakly dependent on the angle between the magnetic field and the axes of the zero field tensor, are observable in powder spectra. Moreover, several Kramers doublets may be involved (*13*). The lines at $g = 4.9$ and $g = 15.8$ are therefore likely due to Fe^{3+} ($S = \frac{5}{2}$) in strongly distorted sites. In addition, intermediate spin configuration (Fe^{3+}, $S = \frac{3}{2}$) might also contribute to the spectrum since it can give rise to lines at g between 0 and 6 (*15*).

These results thus confirmed that significant oxidation was induced by annealing in air. Fe^{3+} ions appear in three types of site at least, probably with tetrahedral, octahedral, and lower symmetry, respectively.

In their ESR investigations of the structurally related compound $CaFeAl_{11}O_{19}$, Glasser *et al.* (*16*) also attribute the broad
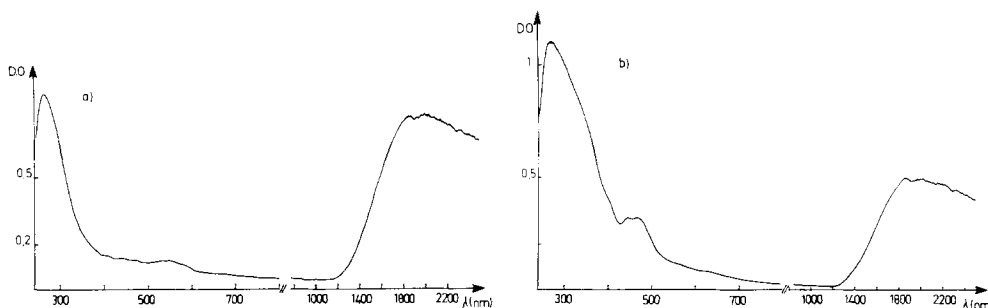
FIG. 3. Diffuse reflectance spectra of LaFeAl$_{11}$O$_{19}$, as-grown (a) and annealed in air at 1500°C (b).

$g \sim 2$ line to magnetically interacting Fe^{3+} ions while transitions in the $g \sim 5.6$ region and low field lines are associated with tetrahedral $S = \frac{3}{2}$ iron ions. This is in good agreement with our assignments of the lines in the LaFeAl$_{11}$O$_{19}$ spectrum although the g values are slightly different for the two compounds.

Diffuse Reflectance Spectra

Diffuse reflectance spectra were obtained at room temperature using a Beckmann 5270-UV spectrophotometer equipped with an integrating sphere. The spectra were referenced against BaSO$_4$.

The spectrum of as-grown LaFeAl$_{11}$O$_{19}$ (Fig. 3a) exhibits a strong broadband in the near-infrared region centered at about 2000 nm with maxima near 1870 and 2020 nm, and a strong band in the near-UV region at 260 nm. Slight modulations also appear in the baseline, in the visible region.

The band at 2000 nm (5000 cm^{-1}) is assigned to tetrahedrally coordinated Fe^{2+} (^5E $\rightarrow$ $^5T_2$ transition). In regular T_d symmetry, the energy is equal to 10 Dq (*17*), giving Dq = 500 cm^{-1}. Tetrahedral coordination is rarely found in minerals, but it is frequent in Fe^{2+} complexes; they usually absorb in the range 3000–7000 cm^{-1} (*17*). On the other hand, octahedral coordination gives only one transition $^5T_{2g} \rightarrow$ ^5E_g; the ^5E_g state gives rise to the Jahn Teller effect and splits

into two sublevels. Two bands are therefore expected: for Fe(H$_2$O)$_6^{2+}$ in single crystals, they appear near 9000–10,000 cm^{-1} (1100–1000 nm). Powdered LaFeAl$_{11}$O$_{19}$ shows no features in this region.

The band at 260 nm (38,462 cm^{-1}) is assigned to the charge transfer O^{2-} $\rightarrow$ Fe^{3+}. The position is the same as in the spectra of a wide variety of oxides, such as Al$_2$O$_3$ (*18*), where it is attributed to traces of Fe^{3+} which may also be responsible for the weak features observed in the visible region.

The spectrum obtained after annealing is shown in Fig. 3b. It is characterized by

(i) the Fe^{2+} band in the IR region, with decreased intensity;

(ii) the charge transfer band at 260 nm, with increased intensity, which shows that some Fe^{2+} has been converted into Fe^{3+};

(iii) two additional bands, rather well-defined and strong at 446 nm (22,422 cm^{-1}) and 467 nm (21,413 cm^{-1}), and a definite shoulder at 615 nm (16,260 cm^{-1}); they must be assigned to Fe^{3+} since they grow markedly after oxidizing annealing.

It must be pointed out that all d–d transitions of high-spin d^5 Fe^{3+} ($S = \frac{5}{2}$) are spin-forbidden since the ground state is $^6A_1$ for tetrahedral and octahedral coordinations, and all the excited states are spin quartets and doublets. They are therefore less intense than for Fe^{2+}. Evaluation of the pro-
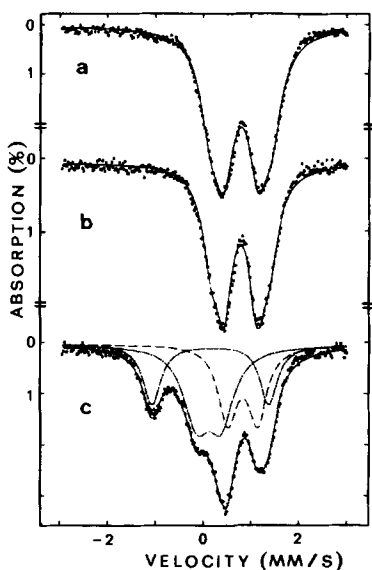
FIG. 4. Room-temperature Mössbauer spectra of as-grown $LaFeAl_{11}O_{19}$ (a), $LaFe_{0.5}Mg_{0.5}Al_{11}O_{19}$ (b), and $LaFeAl_{11}O_{19}$ after annealing in air at 1500°C (c).

portions of Fe^{2+} and Fe^{3+} from the optical density is thereby not reliable.

No feature appears in the region near 24,000 cm^{-1} (417 nm) expected for d–d transitions of octahedrally coordinated Fe^{3+} (19), but such transitions are generally 10 times weaker than for tetrahedral coordination since they are both spin- and parity-forbidden.

The band at 446 nm (22,422 cm^{-1}) is assigned to the $^6A_1$ (^6S) → $^4A_1$, ^4E (^4G) transition which is independent of the crystal field (17). It occurs at the same position in the spectra of many minerals (20) with tetrahedrally coordinated Fe^{3+}. The shoulder at 615 nm (16,260 cm^{-1}) may be due to the $^6A_1$ → $^4T_1$ (^4G) transition (20) which is the first possible transition for Fe^{3+} in tetrahedral site (17). The assignment of the band at 467 nm (21,413 cm^{-1}) is uncertain. It may correspond to the $^6A_1$ → $^4T_2$ (^4G) transition of tetrahedrally coordinated Fe^{3+}, but it would be expected near 20,000 cm^{-1} (20). It may also result from electronic transitions

within Fe^{3+}–Fe^{3+} pairs (21) or from intermediate spin configuration ($S = \frac{3}{2}$) leading to spin-allowed and thereby more intense optical transitions.

The optical study therefore shows that Fe^{2+} is tetrahedrally coordinated in LaFe $Al_{11}O_{19}$, and that it significantly converts into Fe^{3+} by thermal oxidation in air. Fe^{3+} tetrahedral coordination is clearly established but octahedral coordination cannot be ruled out confidently, and assignment of a d–d band remains ambiguous.

Mössbauer Spectra

Mössbauer spectra were recorded at room temperature with a conventional ELSCINT–INEL spectrometer, using a $^{57}Co/Rh$ source. Velocity calibration was made using an α-Fe absorber.

The spectrum of $LaFeAl_{11}O_{19}$ (Fig. 4a) is a broad quasisymmetric quadrupole pattern with isomer shift typical of Fe^{2+} ions; there is no indication of Fe^{3+}. A slight narrowing is observed for $LaFe_{0.5}Mg_{0.5}Al_{11}O_{19}$ (Fig. 4b). The results of least-square fits to two independent doublets are given in Table V. Dilution leads to decreasing quadrupole splittings and linewidths; it suggests a spread in electric field gradients due to a statistical fluctuation of neighboring cations (Fe, Mg, Al, vacancy), rather than a system of two distinct crystallographic sites. The isomer shift of 0.87 mm/sec is consistent with tetrahedral coordination (22); for octahedral coordination, it would be expected beyond 1.1 mm/sec. The parameter values are close to those of Fe^{2+} in the tetrahedral sites of the spinel $FeAl_2O_4$ (23), partially inverse.

The spectrum of the air-annealed material is shown in Fig. 4c. It was fitted to three quadrupole-split doublets, assigned to three distinct sites (Table V). Site 1 still corresponds to Fe^{2+} ions in tetrahedral environment, with somewhat reduced asymmetry. The isomer shift (0.2 mm/sec) of sites 2 and

TABLE V

MÖSSBAUER PARAMETERS OF LaFeAl$_{11}$O$_{19}$ MATERIALS

Sample	Component	IS (mm/sec)	QS (mm/sec)	Γ (mm/sec)	A
LaFeAl$_{11}$O$_{19}$	1	0.87(1)	0.72(1)	0.53(2)	0.64
	2	0.87(1)	1.30(2)	0.50(2)	0.36
LaFe$_{0.5}$Mg$_{0.5}$Al$_{11}$O$_{19}$	1	0.86(1)	0.69(1)	0.41(1)	0.59
	2	0.86(1)	1.22(2)	0.46(2)	0.41
LaFeAl$_{11}$O$_{19}$	1	0.90(1)	0.62(1)	0.47(1)	0.33
annealed in air	2	0.19(1)	0.52(1)	0.66(2)	0.42
at 1530°C	3	0.23(1)	2.44(1)	0.45(1)	0.25

Note. IS, isomer shift with respect to αFe; QS, quadrupole splitting; Γ, line width; A, relative area.

3 is typical of Fe^{3+} (22). Site 2 parameters are characteristic of tetrahedral coordination. Notable line broadening indicates a fluctuating environment. The isomer shift of site 3 falls in the range between octahedral and tetrahedral coordinations, but the quadrupole splitting (2.44 mm/sec) is unusually large. Similar sets (IS, QS) have been reported for Fe^{3+} in highly anisotropic environment, in strongly distorted octahedron in K$_2$NiF$_4$-type structures (24), in five coordination in organic materials (15), in trigonal bipyramid in Fe$_3$PO$_7$ (25), and in hexagonal ferrites (26–28) and Ca-aluminates (16) isotypic with magnetoplumbite. Hence, by analogy, component 3 (Table V) is assigned to Fe^{3+} ions in the Al$_5$ bipyramidal site (Fig. 1).

The large value of the quadrupole splitting may also be related to intermediate spin configuration (15, 24). In the ferrites, however, Fe^{3+} is in the high-spin state. The electronic ground state (^6S) is spherically symmetric; any electric field gradient therefore arises solely from external charges either by direct contribution or by indirect polarization. The latter is the leading feature in BaFe$_{12}$O$_{19}$ (26, 29): 80% of the splitting are accounted for by anisotropic covalency involving the neighboring Ba atoms in the equatorial plane of the bipyramid. A

similar effect is likely to occur in the La-aluminates.

The dynamical behavior of the bipyramidal ion in the ferrites has been investigated. It is still controversial (30). However, it is generally found that the Fe^{3+} ion jumps among the two pseudotetrahedral sites (4e). It may lie in the mirror plane (2b) at low temperature. Structural refinements and temperature evolution of the Mössbauer spectra would help determine the dynamics in the present case.

The fits indicated no significant amount of Fe^{3+} in octahedral sites. This is in contrast with the Fe^{3+} distribution in CaFe$_x^{3+}$Al$_{12-x}$O$_{19}$ (16), which, in addition, yields parameters close to those of sites 2 and 3.

Assuming identical recoil-free fractions for ^{57}Fe in the various sites, we deduce that 67% of the Fe^{2+} ions in LaFeAl$_{11}$O$_{19}$ were converted into Fe^{3+} ions by air annealing. In the oxidized material, 75% of the iron content (33% Fe^{2+}, 42% Fe^{3+}) still have the tetrahedral coordination, and 25%, as Fe^{3+}, occupy bipyramidal sites.

Discussion

The investigated LaFeAl$_{11}$O$_{19}$ crystals are nonstoichiometric and largely iron deficient. Spectroscopic investigations clearly

establish that iron is in the Fe^{2+} state (Fe^{3+} occurring as traces), and tetrahedrally coordinated. This is also confirmed by the structural refinement which, in addition, indicates also a slight spreading of iron in the octahedral sites. Such a spreading hence appears as a possible effect of anisotropic thermal vibrations, or of deviations from stoichiometry. Accordingly, the La, Al_5, and O sublattices (Table II) may be significantly deficient, as already found in similar materials (4).

For $LaM^{2+}Al_{11}O_{19}$ compounds, divalent ion localization in the tetrahedral sites of the so-called spinel blocks (S) is also found for Mg^{2+}, Mn^{2+}, and Co^{2+} (4), whereas Ni^{2+} occupies both tetrahedral and octahedral sites of the S blocks. This is consistent with the ion distribution in the corresponding MAl_2O_4 spinels, essentially normal or close to random, respectively. Note, however, that Fe^{2+} also appears in the tetrahedral sites in the ferrite $La_{0.7}Na_{0.3}Fe_{12}O_{19}$ (31) even though Fe_3O_4 is an inverse spinel. Aluminates isotypic with magnetoplumbite or β-alumina show a systematic reduction of the effective valence (2.7) of the tetrahedral Al^{3+} ions (10). The same effect, weakened, seems to occur for Fe^{3+} in ferrites (2.8 in $BaFe_{12}O_{19}$) (32). The tetrahedral site thus appears somewhat too large for the trivalent ion, Al^{3+} and to a smaller extent Fe^{3+}, to fit in very well. It may easily accept larger ions. Divalent ions, larger, less charged, and more polarizable than Al^{3+}, lead to a better overlapping over the tetrahedral bonds. This probably helps to stabilize the structure of the La-aluminates.

By annealing $LaFeAl_{11}O_{19}$ in air at 1500°C, Fe^{2+} ions are significantly oxidized. A fraction of the Fe^{3+} ions remains in the tetrahedral sites while the rest appears in bipyramidal sites. The latter sites, identified by Mössbauer spectroscopy, may be responsible for the unassigned lines at $g = 4.9$ and 15.8 in the ESR spectrum and for the band at 467 nm (21,413 cm^{-1}) in the optical spectrum.

The conversion of Fe^{2+} into Fe^{3+} necessarily implies oxygen insertion, in the ratio of one O^{2-} per two Fe^{3+} ions. Since the oxidized material still contains some Fe^{2+}, we may consider that the reaction stopped when all oxygen vacancies were filled in. Taking into account the chemical analysis (Table I), and the valence distribution given in Table V, we obtain for the oxidized material the formula

$$La_{0.88}Fe^{2+}_{0.22}Fe^{3+}_{0.44}Al_{11.20}O_{19},$$

in which 0.16 and 0.28 Fe^{3+} ions are in the bipyramidal (Al_5) and tetrahedral (Al_2) sites, respectively. We have for the raw material

$$La_{0.88}Fe^{2+}_{0.66}Al_{11.20}O_{18.78},$$

where the 0.14 Al vacancies are assumed to be located in the Al_5 sites. The Al_5 site population variation due to annealing, with 0.14 Al vacancies before and 0.16 Fe^{3+} ions after, clearly suggests that the Fe^{3+} ions have filled the vacancies. The net results of the oxidation process therefore seem to be:

(i) completion of the oxygen sublattice with correlative conversion $Fe^{2+} \rightarrow Fe^{3+}$;

(ii) occupation of the vacant bipyramidal sites by Fe^{3+} ions while the remaining Fe^{3+} ions stay in the tetrahedral sites;

(iii) transfer of vacancies from the Al_5 (R block) to the Al_2 (S block) sublattice.

It turns out that the Fe^{3+} ions have a stabilizing role. By occupying the bipyramidal sites left vacant by Al^{3+} ions, they allow removal of all vacancies from the mirror plane, except the La ones. The preference of Fe^{3+} over Al^{3+} for these sites may be electrostatic in origin. Both ions are equally charged, but Fe^{3+} ($3d^5$) is more polarizable than Al^{3+} ($2p^6$); coulombic repulsions with the neighboring La^{3+} ions are therefore weakened. Involvement of Fe^{3+} polariza-

tion is actually supported by the large quadrupole splitting of these sites as mentioned above. Relaxation of the La^{3+}–Al^{3+} repulsions is perhaps responsible for the large off-center shift of the La^{3+} ions (2d → 6h, Table II) that lengthens the La^{3+}–Al^{3+} distance by as much as 0.3 Å (Table III). Moreover, since the charge compensation is achieved in LaM^{2+}Al$_{11}$O$_{19}$, one may expect the stoichiometry to be reached easily. This is not the case under our crystal growth operating conditions; we believe it may be due to energy lowering by La^{3+} and/or Al^{3+} vacancy creation.

Iron can thus play a double role in the La-aluminates:

(i) Fe^{2+} ions, like other divalent ions, stabilize the magnetoplumbite structure by decreasing the amount of vacancies, cationic and anionic, compared to LaAl$_{11}$O$_{18}$. Large crystals of LaAl$_{11}$O$_{18}$ are impossible to obtain and the lattice is highly defective. With Fe^{2+} ions present, even with an amount well below the stoichiometry (0.5–0.6 Fe^{2+}/11 Al^{3+}), vacancies in the mirror plane are less numerous. Lattice distortions are thereby reduced and the overall cohesion of the structure is improved. This is evident from the c/a value that decreases from 3.97 for LaAl$_{11}$O$_{18}$ down to 3.94 for LaFe Al$_{11}$O$_{19}$, compared to 3.92 in the true magnetoplumbite structure.

(ii) Specifically, by oxidizing, Fe^{2+} ions improve the structural stabilization of nonstoichiometric materials. Vacancies in the mirror plane are still reduced: oxygen vacancies are suppressed and vacant bipyramidal sites are filled with Fe^{3+} ions. This suggests that deliberate incorporation of Fe^{2+} and Fe^{3+} ions during the crystal growth might help to reach the stoichiometry.

References

1. L. D. SCHEARER, M. LEDUC, D. VIVIEN, A. M. LEJUS, AND J. THERY, *IEEE J. Quantum Elec-tron.* 22(5), 713 (1986); R. MONCORGE, T. BENYATTOU, D. VIVIEN, AND A. M. LEJUS, *J. Lumin.* 35, 199 (1986).
2. J. M. P. J. VERSTEGEN, *J. Electrochem. Soc.* 121(12), 1624 (1974).
3. D. GOLDBERG, *Rev. Int. Hautes Temp. Refract.* 5, 181 (1968).
4. M. GASPERIN, M. C. SAINE, A. KAHN, F. LAVILLE, AND A. M. LEJUS, *J. Solid State Chem.* 54, 61 (1984).
5. D. SABER AND A. M. LEJUS, *Mater. Res. Bull.* 16, 1325 (1981).
6. G. BLASSE AND A. BRIL, *Philips Res. Rep.* 23, 201 (1968).
7. J. M. P. J. VERSTEGEN, J. L. SOMMERDIJK, AND J. G. VERRIET, *J. Lumin.* 6, 425 (1973).
8. F. LAVILLE AND A. M. LEJUS, *J. Crystal Growth* 63, 426 (1983).
9. I. D. BROWN AND D. ALDERMATT, *Acta Crystallogr. Sect. B* 41, 244 (1985).
10. T. R. WAGNER AND M. O'KEEFFE, *J. Solid State Chem.* 73, 211 (1988).
11. C. S. SUNANDANA AND R. JAGANNATHAN, *Solid State Commun.* 53, 985 (1985).
12. B. CAMARA, *J. Phys.* 43, C9-165 (1982).
13. R. D. DOWSING AND J. F. GIBSON, *J. Chem. Phys.* 50, 294 (1969).
14. LIN FUCHENG, *Sci. Sin. Ser. A* 25, 1298 (1982).
15. D. NIARCHOS, A. KOSTIKAS, A. SIMOPOULOS, D. COUCOUVANIS, D. PILTINGSRUD, AND R. E. COFFMAN, *J. Chem. Phys.* 69, 4411 (1978).
16. F. P. GLASSER, F. W. D. WOODHAMS, R. E. MEADS, AND W. G. PARKER, *J. Solid State Chem.* 5, 255 (1972).
17. A. B. P. LEVER, "Inorganic Electronic Spectroscopy," 2nd ed., Elsevier, Amsterdam (1984).
18. H. H. TIPPINS, *Phys. Rev. B* 1, 126 (1970).
19. A. A. KINAWI, *J. Inorg. Nucl. Chem.* 43, 1989 (1981).
20. A. M. HOFMEISTER AND G. R. ROSSMAN, *Phys. Chem. Miner.* 11, 213 (1984).
21. D. M. SHERMAN AND T. D. WAITE, *Amer. Mineral.* 70, 1262 (1985).
22. F. MENIL, *J. Phys. Chem. Solids* 46, 763 (1985).
23. C. M. YAGNIK AND H. B. MATHUR, *J. Phys. C, Ser. 2,* 469 (1968).
24. G. DEMAZEAU, M. POUCHARD, M. THOMAS, J. F. COLOMBET, J. C. GRENIER, L. FOURNES, J. L. SOUBEYROUX, AND P. HAGENMULLER, *Mater. Res. Bull.* 15, 451 (1980).
25. A. MODARESSI, A. COURTOIS, R. GERARDIN, B. MALAMAN, AND C. GLEITZER, *J. Solid State Chem.* 47, 245 (1983).
26. E. KREBER, U. GONSER, A. TRAUTWEIN, AND F. E. HARRIS, *J. Phys. Chem. Solids* 36, 263 (1975).
27. X. OBRADORS, J. TEJADA, A. ISALGUE, AND J. C. JOUBERT, *Solid State Commun.* 50, 821 (1984).

28. M. C. CADEE AND D. J. W. IJDO, *J. Solid State Chem.* **52**, 302 (1984).

29. A. TRAUTWEIN, E. KREBER, U. GONSER, AND F. E. HARRIS, *J. Phys. Chem. Solids* **36**, 325 (1975).

30. J. FONTCUBERTA, A. ISALGUE, AND X. OBRADORS, *Z. Phys. B* **70**, 370 (1988).

31. D. LE ROUX, H. VINCENT, J. C. JOUBERT, AND M. VALLET-REGI, *Mater. Res. Bull.* **23**, 299 (1988).

32. X. OBRADORS, A. COLLOMB, M. PERNET, D. SAMARAS, AND J. C. JOUBERT, *J. Solid State Chem.* **56**, 171 (1985).